Xu *et al.*
Chinese Journal of Mechanical Engineering (2022) 35:93
https://doi.org/10.1186/s10033-022-00758-5

Chinese Journal of Mechanical Engineering

ORIGINAL ARTICLE

Open Access

Uncertainty Analysis and Optimization of Quasi-Zero Stiffness Air Suspension Based on Polynomial Chaos Method

Xing Xu*, Huan Liu, Xinwei Jiang and Akolbire Vincent Atindana

Abstract

To improve the vibration isolation performance of suspensions, various new structural forms of suspensions have been proposed. However, there is uncertainty in these new structure suspensions, so the deterministic research cannot reflect the performance of the suspension under actual operating conditions. In this paper, a quasi-zero stiffness isolator is used in automotive suspensions to form a new suspension—quasi-zero stiffness air suspension (QZSAS). Due to the strong nonlinearity and structural complexity of quasi-zero stiffness suspensions, changes in structural parameters may cause dramatic changes in suspension performance, so it is of practical importance to study the effect of structural parameter uncertainty on the suspension performance. In order to solve this problem, three suspension structural parameters d_0, L_0 and P_{c0} are selected as random variables, and the polynomial chaos expansion (PCE) theory is used to solve the suspension performance parameters. The sensitivity of the performance parameters to different structural parameters was discussed and analyzed in the frequency domain. Furthermore, a multi-objective optimization of the structural parameters d_0, L_0 and P_{c0} of QZSAS was performed with the mean and variance of the root-mean-square (RMS) acceleration values as the optimization objectives. The optimization results show that there is an improvement of about 8%—10% in the mean value and about 40%—55% in the standard deviation of acceleration (RMS) values. This paper verifies the feasibility of the PCE method for solving the uncertainty problem of complex nonlinear systems, which provide a reference for the future structural design and optimization of such suspension systems.

Keywords: Air suspension, Quasi-zero stiffness, Polynomial chaos, Uncertainty analysis, Optimization

1 Introduction

The suspension system is an essential part of automobiles assembly, which affects ride comfort, handling stability and driving safety. In order to improve the suspension performance, various new structures for suspensions have been proposed. The suspension serves as a vibration isolation system, and much of its structural design depends on the type of vibration isolator. A quasi-zero stiffness isolator is a nonlinear vibration isolation system with high static stiffness and low dynamic stiffness [1, 2]. Alabuzhev and Gritchin first put forward the concept of quasi-zero stiffness [3]. And the basic principle of quasi-zero stiffness realization is to introduce a negative stiffness structure into a positive stiffness system [4, 5]. Through theoretical and experimental analysis, some scholars proved that the system has a larger vibration isolation frequency range and higher vibration attenuation rate compared with the system without negative stiffness [6, 7]. Although the quasi-zero stiffness isolator has attracted much attention from scholars because of its excellent vibration isolation performance, few scholars have applied it to suspensions and studied the influence of structural parametric uncertainty on its performance.

*Correspondence: xuxing@ujs.edu.cn

Automotive Engineering Research Institute, Jiangsu University, Zhenjiang 212013, China

Springer Open

© The Author(s) 2022. **Open Access** This article is licensed under a Creative Commons Attribution 4.0 International License, which permits use, sharing, adaptation, distribution and reproduction in any medium or format, as long as you give appropriate credit to the original author(s) and the source, provide a link to the Creative Commons licence, and indicate if changes were made. The images or other third party material in this article are included in the article's Creative Commons licence, unless indicated otherwise in a credit line to the material. If material is not included in the article's Creative Commons licence and your intended use is not permitted by statutory regulation or exceeds the permitted use, you will need to obtain permission directly from the copyright holder. To view a copy of this licence, visit http://creativecommons.org/licenses/by/4.0/.

Generally, vehicle parameters are considered as deterministic, but in fact there are still many uncertain parameters, which can be made by design tolerance, manufacture error, and/or time-varying, which greatly affect vehicle dynamic performance. It is very important to consider the parametric uncertainty in the analysis of suspension performance [8, 9]. Nagy and Braatz classified uncertainty propagation methods available into three categories: (i) analytical methods, (ii) Monte Carlo simulation methods, and (iii) response surface methods, and stated that analytical methods are the most efficient [10]. The most accurate of these is Monte Carlo (MC) simulation, but this often requires thousands of deterministic simulations to obtain uncertainty statistics, which is infeasible for computationally expensive CFD simulations [11]. Dai et al. applied MC method to the field of automobile suspension [12]. Chen et al. used MC simulation results to verify the correctness of the application of unascertained theory in automobile suspension [13].

An alternative approach, which has been intensively applied in the past decades, is based on stochastic response surface (SRS). It describes the performance function/model output as a sum of elementary functions of stochastic input parameters. Polynomial chaos expansion (PCE) as a functional approximation of the mathematical model belongs to the class of SRS approaches. PCE method was first proposed by Wiener [14]. It was mainly used to establish turbulence model. Now, PCE method has been widely used in many engineering fields, such as fluid mechanics [11], structural dynamics systems [15], controller design [16], multibody dynamics [17], aerospace technology [18] and power systems [19]. Many researchers found that the computational burden of the polynomial chaos expansion-based approach is significantly lower than that of the MC approach [11, 20, 21].

In the past decades, air springs have been widely used in commercial vehicles because of their advantages of reducing weight, adjusting ride height, improving driving comfort, reducing road damage and structural noise [22, 23]. In this paper, a new type of automotive suspension, quasi-zero stiffness air suspension (QZSAS), was proposed. The uncertainty of the parameters on suspension performance was analyzed using polynomial chaos expansion theory. Then, the statistical properties of QZSAS performance were taken as the objective function of optimization, which is a typical Pareto optimization problem [24, 25]. Genetic algorithm, which is widely used for passive and semi-active suspension optimization [26–28], is adopted to perform a multi-objective optimization of QZSAS with considering parameter uncertainty. To verify the effectiveness of proposed method, a bench testing for model validation and optimization simulation is carried out.

2 Quasi-Zero Stiffness Air Suspension System

2.1 Mechanical Analysis

The QZSAS studied in this paper is a suspension for commercial vehicles. The mechanism is supported in the vertical direction by an air spring to provide positive stiffness. Two horizontally opposed cylinders are mounted on either side of the air spring for the purpose of providing negative stiffness. The stiffness of the system is the sum of the two stiffnesses. The negative stiffness can be changed by adjusting the air pressure of the cylinders, which can make the system stiffness near the equilibrium position approximately zero, when the load is constant. However, in practical applications, the total system stiffness will not be zero but slightly greater than zero in order to ensure the stability of the system.

As shown in Figure 1, pressurized air in the cylinders and air spring is supplied by the high-pressure air tank, and the discharged air goes to the low-pressure air tank. As with conventional suspensions, shock absorbers are installed between the body and the frame, and the frame is connected to the wheels (not shown in Figure 1).

When the vehicle is driven on a bumpy road, the body and frame will be displaced relatively to each other, the air spring will be stretched or compressed, and the cylinders will rotate as shown in Figure 2.

Since the quasi-zero stiffness air suspension uses the compressibility of air to produce vibration isolation. The relationship between air pressure and volume in air spring and cylinders will be given by the gas state equation in Eq. (1), where the sprung mass is considered to be constant.

$$PV^n = P_0 V_0^n, \tag{1}$$

where P_0 is the initial state air pressure, V_0 is the initial state volume, P is the air pressure in any state, V is the volume in any state, and n is the polytropic index.

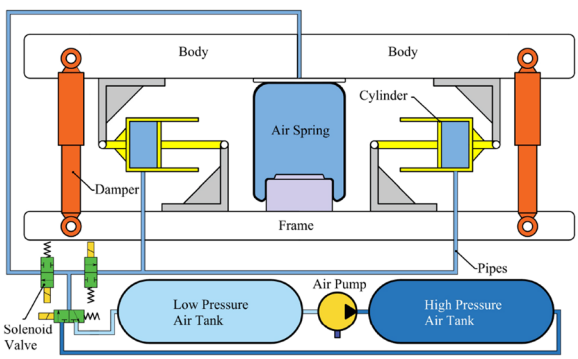

Figure 1 Structure of quasi-zero stiffness air suspension

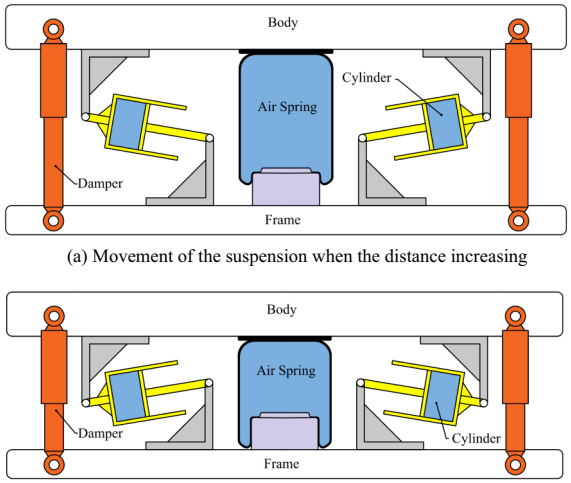

(a) Movement of the suspension when the distance increasing

(b) Movement of the suspension when the distance decreasing

Figure 2 Suspension movement when the distance between the bod and the frame changing

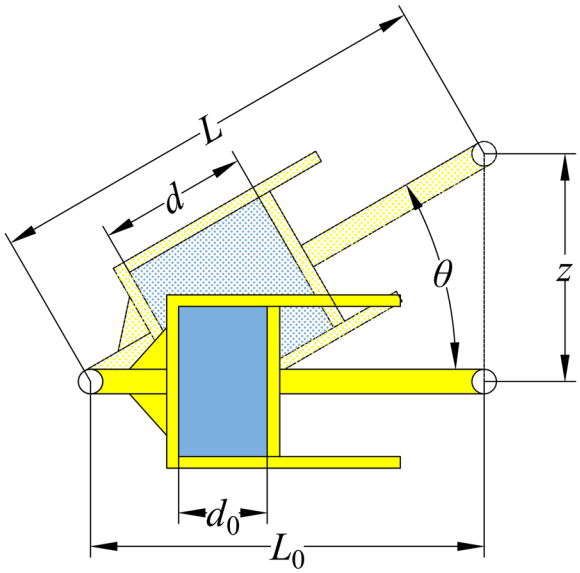

Figure 3 Geometric relationship of cylinder motion

The air spring selected is a diaphragm air spring. In its working air pressure range. During its effective area is almost unchanged. It will be simplified to a cylinder with constant piston area. For a certain displacement z, according to the gas state Eq. (1), the size of its force as shown in Eq. (2):

$$F_s = A_s\left[P_{s0}\left(\frac{z_0}{z_0 - z}\right)^{n_s} - P_a\right], \tag{2}$$

where A_s is the effective area of air spring, P_{s0} is the air spring pressure in the equilibrium position, z_0 is the height of air spring in the equilibrium position, and P_a is the atmospheric pressure.

Figure 3 shows the movement of left cylinder when the vehicle driving on the bumpy road. d_0 is the distance from the piston to the back wall of the higher-pressure chamber and L_0 is the distance between the two hinge points of the cylinder when the vehicle is stationary. When the relative displacement occurs, the cylinder will rotate. θ is the cylinder rotation angle, z is the displacement of the body relative to the frame, d is the distance from the piston to the back wall of the high-pressure chamber and L is the distance between the two hinge points of the cylinder when the vehicle is in motion. The geometric relationship of these parameters and variables can be given by Eqs. (3) (4) and (5):

$$L = \sqrt{L_0^2 + z^2}, \tag{3}$$

$$\sin\theta = \frac{z}{\sqrt{L_0^2 + z^2}}, \tag{4}$$

$$\Delta d = \sqrt{\left(L_0^2 + z^2\right)} - L_0. \tag{5}$$

Then, through mechanical analysis, the fore of negative stiffness cylinder in the vertical direction can be given by Eq. (6):

$$F_c = 2A_c\left[P_{c0}\left(\frac{d_0}{d_0 + \Delta d}\right)^{n_c} - P_a\right]\sin\theta, \tag{6}$$

where A_c is the effective area of the cylinder, P_{c0} is the cylinder equilibrium position air pressure, and n_c is the gas polytropic index inside the cylinder.

$$\begin{cases} m_1\ddot{z}_1 + C(\dot{z}_1 - \dot{z}_2) - F = 0, \\ m_2\ddot{z}_2 - C(\dot{z}_1 - \dot{z}_2) + K_t(z_2 - q) + F = 0. \end{cases} \tag{7}$$

After determining the forces provided by the positive and negative stiffnesses system, the dynamic equations of the system can be given by Eq. (7) according to the quasi-zero stiffness 1/4 air suspension model shown in Figure 4. Where C is the damping coefficient and K_t is the tire stiffness. The F value can be obtained from Eq. (8):

$$F = F_s(z_1 - z_2) + F_c(z_1 - z_2) - m_1 g, \tag{8}$$

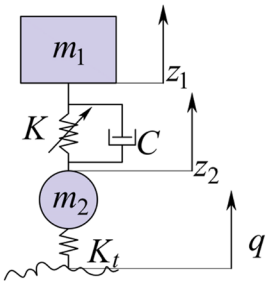

Figure 4 Simplification of 1/4 quasi-zero stiffness air suspension

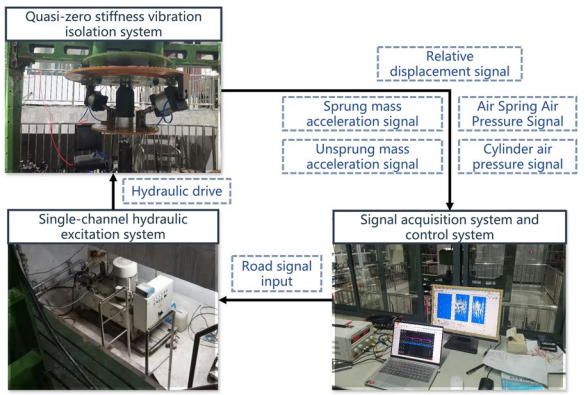

Figure 5 Experimental setup of QZSAS

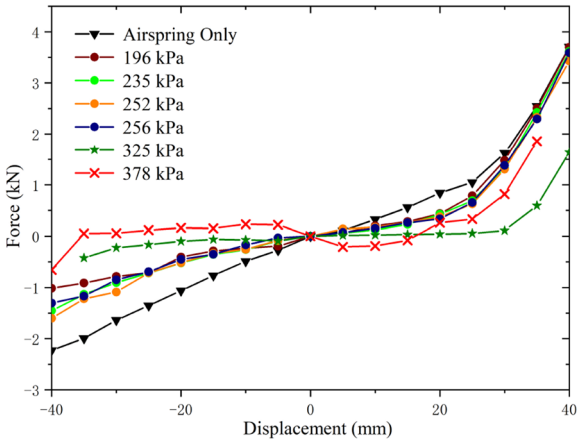

Figure 6 Static characteristics of QZSAS at different air pressures of negative stiffness

Table 1 Dynamic characterization experiment

Group	Load (kg)	P_{s0} (kPa)	P_{c0} (kPa)	Frequency (Hz)
1	690	255	—	0.2, 0.4,…, 5, 6, 7, 8, 9
2	800	280	—	
3	690	255	250	
4	690	255	330	
5	800	280	330	

where $F_s(z_1 - z_2)$ is a function of the distance $(z_1 - z_2)$ between the body and frame, and similarly for $F_c(z_1 - z_2)$. These two can be calculated separately by Eqs. (2) and (6).

2.2 Experiment and Validation

Figure 5 shows the construction of the test bench for the QZSAS. This servo system consists mainly of a hydraulic cylinder, controlled by a servo valve and controller. A single channel servo-hydraulic system is used to create various ideal excitations such as sinusoidal excitation. Two sets of tests are conducted, static and dynamic experiments.

For static experiment, Air spring pressure is set at 155 kPa and the spring mass is 690 kg. Cylinder air pressure increased from 196 to 378 kPa. Figure 6 shows the mechanical characteristics of QZSAS at different air pressures, it can be seen that as the air pressure of negative stiffness system increases, the curve changes more and more gently. Static experiments show that it is feasible to change the stiffness of the whole system by changing the air pressure of the cylinder, and the whole system can reach quasi zero stiffness.

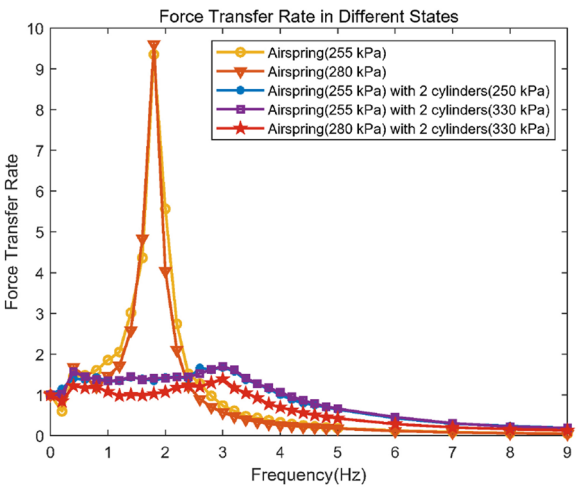

Figure 7 Force transmissibility of QZSAS and air spring

In order to further study the vibration isolation performance of QZSAS, each frequency response test was conducted, and the test items are shown in Table 1. Figure 7 shows the suspension force transfer rate. It can be clearly seen that the vibration isolation performance

of QZSAS is better than that of air spring in the low frequency band, and no obvious resonance peak will appear. At the same time, as the load increases, the vibration isolation performance of QZSAS becomes better than that of air spring. Therefore, it can be seen that the performance of QZSAS is better than that of the ordinary suspension with air spring only.

3 Uncertainty Modeling Base on PCE

3.1 Polynomial Chaos Expansion Method

The PCE method is actually an alternative model approach. For a complex model of a sufficiently smooth black-box system in probability space, as represented by Eq. (9):

$$\boldsymbol{Y} = f(\boldsymbol{X}), \tag{9}$$

where $\boldsymbol{X}$ is the input to the black box and $\boldsymbol{Y}$ is the output of the black box, but the correspondence is not known. Usually, black box systems are highly nonlinear and difficult to express in explicit terms. The essence of polynomial chaos expansion is to approximate this black box by a set of polynomials. This alternative model can be expressed as Eq. (10):

$$\begin{aligned} Y = c_0 + \sum_{i_1=1}^{n} c_{i_1}\Gamma_1(\xi_{i_1}) + \sum_{i_1=1}^{n}\sum_{i_2=1}^{i_1} c_{i_1 i_2}\Gamma_2(\xi_{i_1},\xi_{i_2}) \\ + \sum_{i_1=1}^{n}\sum_{i_2=1}^{i_1}\sum_{i_3=1}^{i_2} c_{i_1 i_2 i_3}\Gamma_3(\xi_{i_1},\xi_{i_2},\xi_{i_3})\cdots \end{aligned} \tag{10}$$

where c_i is the coefficient to be solved; ξ_i is the uncertainty variable obeying the standard normal distribution; $\Gamma_i(\boldsymbol{\xi})$ is Hermite orthogonal polynomial, whose general formula can be expressed as Eq. (11):

$$\Gamma_{dim}(\boldsymbol{\xi}) = (-1)^{dim} e^{\frac{1}{2}\boldsymbol{\xi}^{\mathrm{T}}\boldsymbol{\xi}} \frac{\partial^{dim}}{\partial\xi_{i_1},\cdots,\partial\xi_{i_{dim}}} e^{-\frac{1}{2}\boldsymbol{\xi}^{\mathrm{T}}\boldsymbol{\xi}}, \tag{11}$$

where *dim* is the number of random variable dimensions. And the $\boldsymbol{\xi} = [\xi_{i1}, \xi_{i2}, ..., \xi_{idim}]$.

In practical applications, it is not possible to expand the polynomial by an infinite number of terms. Usually the s-term truncation is taken to approximate the system output, and the above equation can be approximated in the form of Eq. (12):

$$Y \approx \sum_{i=0}^{s-1} c_i\Gamma_i(\xi). \tag{12}$$

The recursive formula will be used instead of the defining equation of Eq. (11), which facilitates the procedural implementation of the chaotic polynomial, and the recursive formula is shown in Eq. (13). Here i is the order of the Hermite polynomial.

For computational convenience, the Hermite polynomials are normalized by dividing each term by the square root of the factorial of the order. The Hermite polynomials after normalization of the first 6 orders are given by Table 2.

$$\begin{cases} \Gamma_1(\xi) = 1, \\ \Gamma_2(\xi) = \xi, \\ \Gamma_i(\xi) = \xi\,\Gamma_{i-1}(\xi) - (i-2)\Gamma_{i-2}(\xi)\ (i>3). \end{cases} \tag{13}$$

The solution of the polynomial chaos coefficients c_i is a crucial step. In general, the solution of the coefficients can be classified as intrusive or non-intrusive. For the black-box problem, it is not easy to use the invasive solution because the specific expression of the initial model cannot be determined, so the noninvasive method is chosen to calculate the coefficients. There are two commonly used methods for non-invasive solutions, the Galerkin projection method and the collection method. The collection method is easier to implement than the Galerkin method, especially for nonlinear systems [29], and this paper used the collection method for solving the polynomial chaotic coefficients.

The key step is to select and combine the collocation points. For the random variables obeying Gaussian stochastic process, the expansion base should be chosen as Hermite orthogonal polynomial. Assuming that the order of expansion is m, then the collocation points can be chosen as the roots of $(m+1)$th Hermite orthogonal polynomials [30]. The collocation points cannot be directly input to the system, therefore, they need to be transformed into input variables. Taking a random variable obeying Gaussian distribution as an example, the input variable $x = \sigma\xi+\mu$, where μ, σ are the prior mean and standard deviation of the input random variables. The process of calculating the output response statistics using the PCE method is shown in Figure 8.

If only collocation points obtained by finding the roots of the polynomial are selected for the calculation, it may lead to inaccurate calculation of the coefficients.

Table 2 The normalized Hermite polynomials

Polynomial Order	Hermite polynomials
0th	1
1st	ξ
2nd	$\frac{1}{\sqrt{2}}\left(\xi^2-1\right)$
3rd	$\frac{1}{\sqrt{6}}\left(\xi^3-3\xi\right)$
4th	$\frac{1}{2\sqrt{6}}\left(\xi^4-6\xi^2+3\right)$
5th	$\frac{1}{2\sqrt{30}}\left(\xi^5-10\xi^3+15\xi\right)$

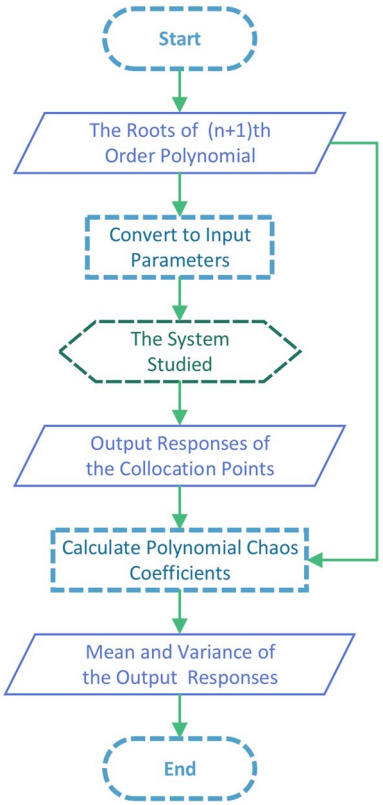

Figure 8 Process for calculating output response statistics using the PCE method

In order to minimize the influence of each group of collocation points on the response surface, more collocation points can be introduced to solve the coefficients. The number of groups of collocation points is only needed to be more than the total number of coefficients to be solved, and the polynomial coefficients can be obtained by solving the system of linear equations shown in Eq. (14):

$$\begin{bmatrix} \Gamma_0(\xi_0) & \Gamma_1(\xi_0) & \cdots & \Gamma_{s-1}(\xi_0) \\ \Gamma_0(\xi_1) & \Gamma_1(\xi_1) & \cdots & \Gamma_{s-1}(\xi_1) \\ \vdots & \vdots & & \vdots \\ \Gamma_0(\xi_N) & \Gamma_1(\xi_N) & \cdots & \Gamma_{s-1}(\xi_N) \end{bmatrix} \begin{bmatrix} c_0 \\ c_1 \\ \vdots \\ c_{s-1} \end{bmatrix} = \begin{bmatrix} Y(\xi_0) \\ Y(\xi_1) \\ \vdots \\ Y(\xi_N) \end{bmatrix}, \tag{14}$$

where N is the total number of sampling points, and s is the number of coefficients to be solved.

Since the orthogonal polynomial has the property of weighted orthogonality, its mean and variance can be found more quickly from the coefficients of the chaotic polynomial. Eq. (15) is the mean solution of the system response Y. Eq. (16) is the variance solution of the system response Y. The first coefficient of the polynomial is the mean of the response, and the sum of the squares of the coefficients from the second term to the last term is the variance of the response. After the PCE model is obtained, the statistical distribution of the response can be found by bringing in the alternative model using MC method for sampling:

$$\mu_Y = \int_\Omega g(\xi) f(\xi) \mathrm{d}\xi = c_0, \tag{15}$$

$$\sigma_Y^2 = \int_\Omega g^2(\xi) f(\xi) \mathrm{d}\xi - \mu_Y^2 = \sum_{i=1}^{s-1} c_i^2, \tag{16}$$

where $g(\xi)$ is a function of the polynomial alternative model and $f(\xi)$ is the power function of the polynomial expansion.

Table 3 Parameters of QZSAS

Parameters	Value
Air polytropic index n_s, n_c	1
Cylinder node distance L_0 (m)	0.467
Distance between cylinder piston and end face d_0 (mm)	32
Cylinder piston area A_c (m^2)	0.0314
Effective area of air spring A_s (m^2)	0.0421
Shock absorber damping factor C (N·s/m)	2000
Wheel mass m_2 (kg)	100
Body mass m_1 (kg)	800
Tire stiffness K_t (N/m)	243000
Initial height of air spring z_0 (m)	0.275
Air spring initial air pressure P_{s0} (kPa)	288
Cylinder initial air pressure P_{c0} (kPa)	300

3.2 Using PCE on the QZSAS

The QZSAS in this paper is a strongly nonlinear system whose mathematical model has been presented in previous section. The parameters of the suspension are given in Table 3. n_s, n_c are the air polytropic index of the air spring and cylinder, respectively. d_0, L_0 have the meanings shown in Figure 3, d_0 is the distance between cylinder piston and end face at the state shown in Figure 1. And L_0 is the cylinder node distance. A_c is the piston area of the cylinder, A_s is the effective area of the air spring, C is the damper damping factor of QZSAS, which can be seen in Figures 1, 2, and 4. And the mass of the wheel is denoted as m_2, the mass of the body is denoted as m_1. K_t is the stiffness of a single tire, which can be seen in Figure 4. z_0 is the height of air spring when QZSAS is in the state shown in Figure 1. P_{s0} and P_{c0} are the air pressure of air spring and cylinder, respectively, when the QZSAS is in the state shown in Figure 1. The MATLAB/Simulink based simulation model of QZSAS is established through the data in Table 3.

$$a,f_d,\frac{F_d}{G}\approx\sum_{i=0}^{s-1}c_{pi}\Gamma_i(P_{c0}), \tag{17}$$

$$a,f_d,\frac{F_d}{G}\approx\sum_{i=0}^{s-1}c_{di}\Gamma_i(d_0), \tag{18}$$

$$a,f_d,\frac{F_d}{G}\approx\sum_{i=0}^{s-1}c_{li}\Gamma_i(L_0), \tag{19}$$

The main QZSAS parameters are selected as random variables in this paper. Their magnitudes are taken into account due to manufacturing and installation tolerance, sensor accuracy, equipment errors and other uncertainties. Since the QZSAS has multiple components, errors are inevitable in the manufacturing and installation process. d_0 and L_0 as non-manufacturing quantities, whose magnitudes are determined by other manufacturing quantities, have a wide range of variation due to installation and manufacturing errors, so they were selected as uncertain parameters.

P_{c0} is the air pressure of the cylinder at the balance position of the suspension system. Its value is determined by the delayed effect of the air during inflation, the closing accuracy of the solenoid valve, and the accuracy of the air pressure sensor. Its actual value is inconsistent with the expected size during inflation, and there is a fluctuation range, so P_{c0} was chosen as a parameter of uncertainty analysis.

The above parameters are affected by many mutually independent random factors, and the impact of each factor is very small. These parameters can be seen as obeying a normal distribution, the mean value of d_0, L_0 and P_{c0} is in the Table 3. If the coefficient of variation ζ is taken as 10%, their probability density distribution can be given in Figure 9.

After determining the uncertain parameters, the QZSAS is regarded as a nonlinear black box system, and the Matlab/Simulink based model is used instead. The model can be built from the differential Eq. (7).

The uncertain parameters matching with the standard normal distribution are added into the simulation model. To determine the effect of parameters uncertainties on suspension performance, the body acceleration a, suspension dynamic deflection f_d, and wheel relative dynamic load F_d/G used to evaluate the suspension performance are obtained. The body acceleration a is the main indicator to evaluate the smoothness of the vehicle. The dynamic suspension deflection, which is defined as the relative displacement of the body and the frame, is related to its limit travel. And its improper fit increases the probability of hitting the limit and makes the smoothness worse. The relative dynamic load of the suspension is the ratio of wheel dynamic Load F_d between static load G. Where dynamic load F_d equals to $K_t(z_2-q)$, static load G equals to $(m_1+m_2)g$. The relative dynamic load affects the adhesion effect between the wheel and the road, and is related to driving safety. The expression of polynomial chaos is obtained, as given in Eqs. (17)–(19).

The coefficients of polynomial chaos can be calculated by Eq. (14), and the mean and variance of a, F_d/G, and f_d can be quickly calculated by Eqs. (15) and (16). If further distribution of the output response is desired, the sampling points can be brought into PCE with the help of the MC method.

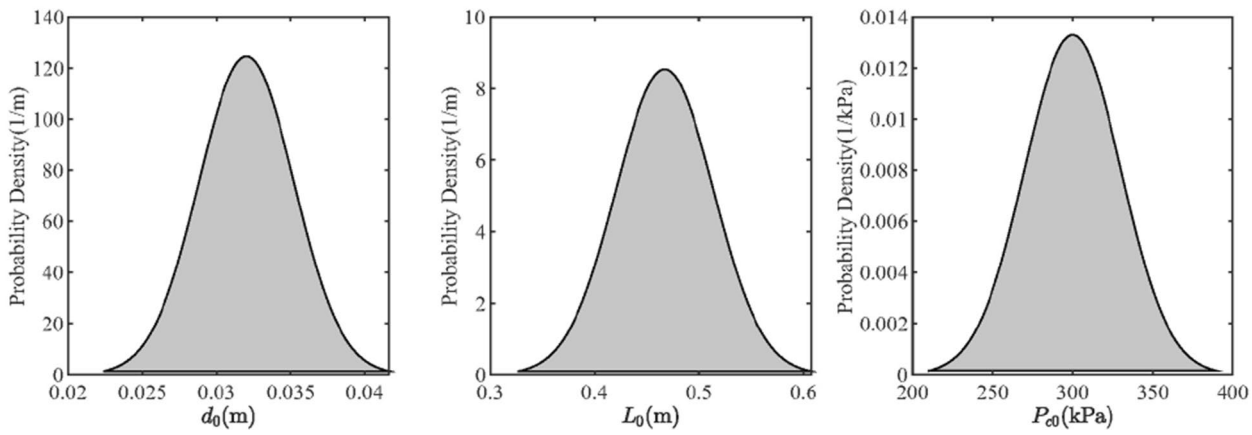

Figure 9 Distribution of random variables with a variance coefficient ($\zeta = 10\%$)

4 Uncertainty Analysis of QZSAS

Three road profile excitations are selected in this paper: sine excitation, step excitation, and full frequency band excitation. For sine excitation, the signal with an amplitude of 0.1 m and frequency 1 Hz was used to do the simulation. For the step excitation, the jump time is the first 1 s, and its amplitude is 0.05 m. Full frequency band excitation consists of a series of sine signals with an amplitude of 0.1 m, the lowest frequency sine signal is 0.1 Hz the largest frequency sine signal is 30 Hz, and the individual sine signals are spaced 0.1 Hz apart. And the statistical index of the output response under each excitation is derived.

For the input of sinusoidal pavement, the coefficient of variation of d_0, L_0 and P_{c0} is 0.1, and their distributions are shown in Figure 9. The corresponding output responses of performance variables are shown in Figures 10, 11 and 12.

It can be seen that in comparison, the uncertainty of P_{c0} has the largest effect on the standard deviation response of sprung mass acceleration, and the effects of d_0 and L_0 on the standard deviation are very close. The effects of three parameters on the mean acceleration response are almost the same. The acceleration distribution at the top is more dispersed compared to that at the bottom.

Figure 11 shows each of three random variables on the dynamic deflection response of the suspension. P_{c0} is still the random variable that affects the standard deviation the most, and the other two random variables do not have very different effects on the standard deviation. The mean values of the deflection responses of three random variables are almost the same.

The effects of P_{c0}, L_0 and d_0 on the dynamic load response of the suspension are given in Figure 12. The effects of three random variables on the mean and variance of the dynamic load response are almost the same as the acceleration and dynamic deflection.

To verify the correctness of the PCE method, a stochastic simulation was carried out using the MC method and compared with the PCE-MC method. The PCE-MC method means that the sampling points are brought into the PCE alternative model rather than into the actual model as in the MC method. The number of the random sampling points selected was 500, and the probability density profile of Figure 13 was obtained after the numerical simulation of the two methods. Where Figures 13(a), (b), (c), show the probability density functions of a, f_d, and F_d/G.

From the Figure 9, it can be seen that the input random variables P_{c0}, L_0 and d_0 are obeying a symmetric normal distribution. As a comparison, from Figure 13, the distributions of the output random variables a, f_d, and F_d/G are not symmetrical but skewed distribution.

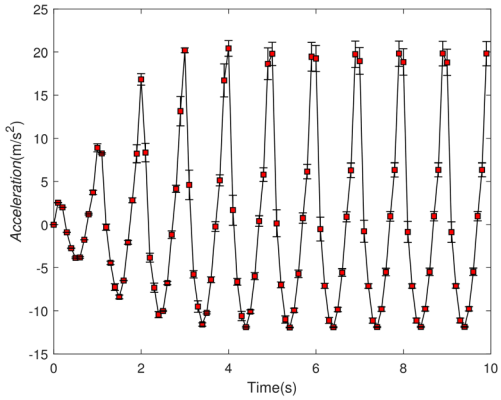

(a) Effect of d_0 on body acceleration

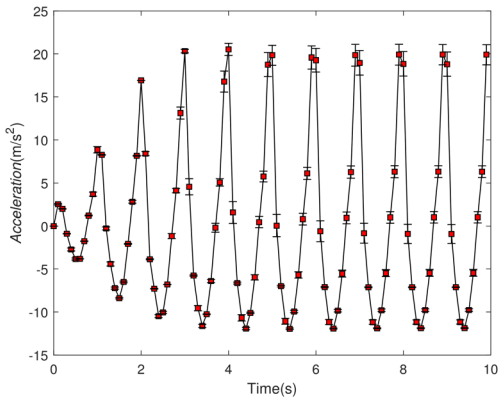

(b) Effect of L_0 on body acceleration

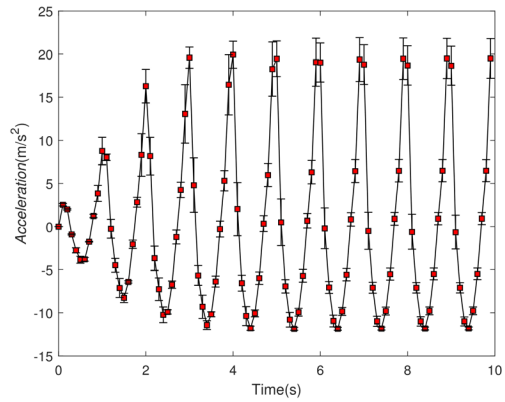

(c) Effect of P_{c0} on body acceleration

Figure 10 Effect of different parameter uncertainties on the mean and standard deviation of body acceleration

The distribution function of the output random variables calculated using the MC method and the PCE-MC method are almost the same. And the MC method is an exact verified random method. It also verifies the feasibility and validity of the PCE-MC method.

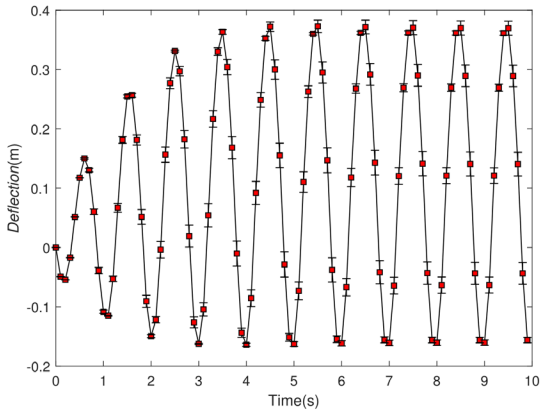

(a) Effect of d_0 on dynamic deflection

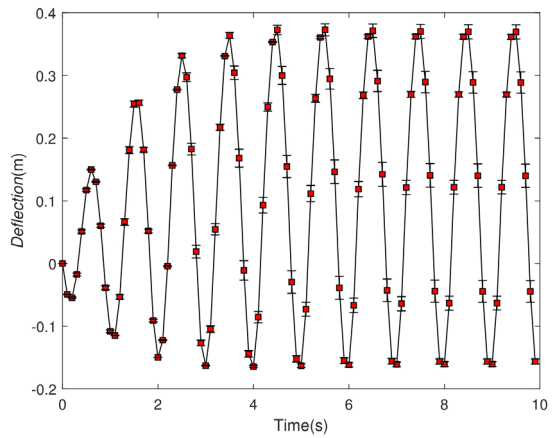

(b) Effect of L_0 on dynamic deflection

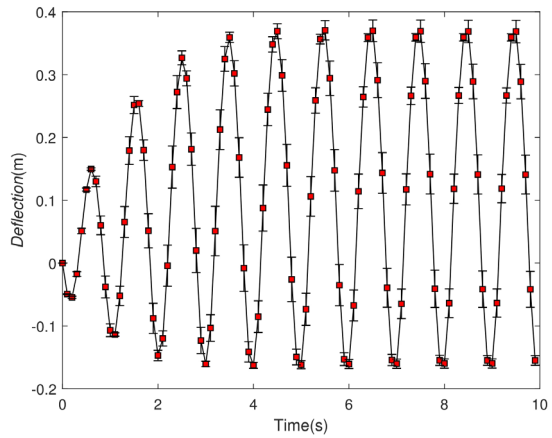

(c) Effect of P_{c0} on dynamic deflection

Figure 11 Effect of different parameter uncertainties on the mean and standard deviation of dynamic deflection

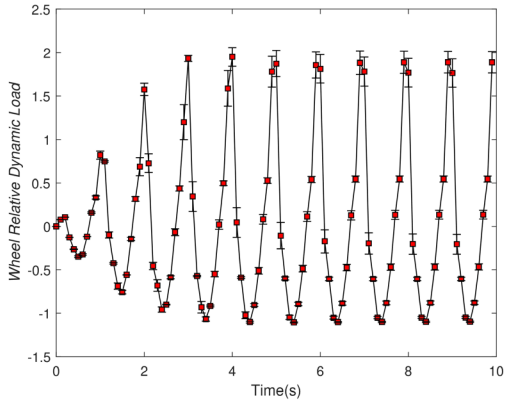

(a) Effect of d_0 on dynamic load

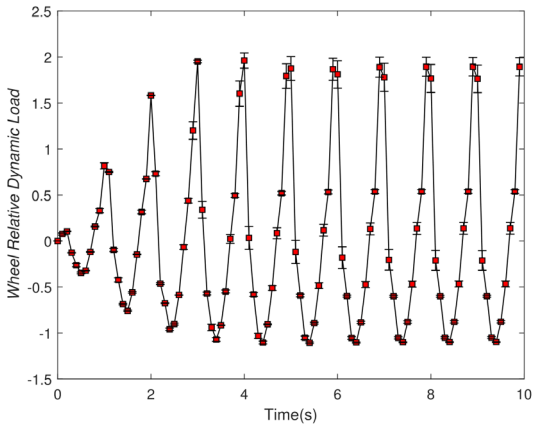

(b) Effect of L_0 on dynamic load

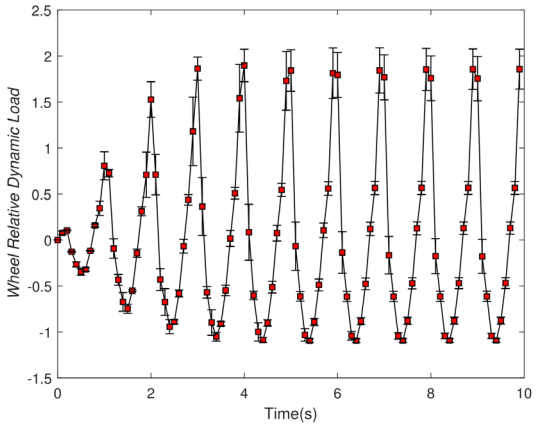

(c) Effect of P_{c0} on dynamic load

Figure 12 Effect of different parameter uncertainties on the mean and standard deviation of dynamic load

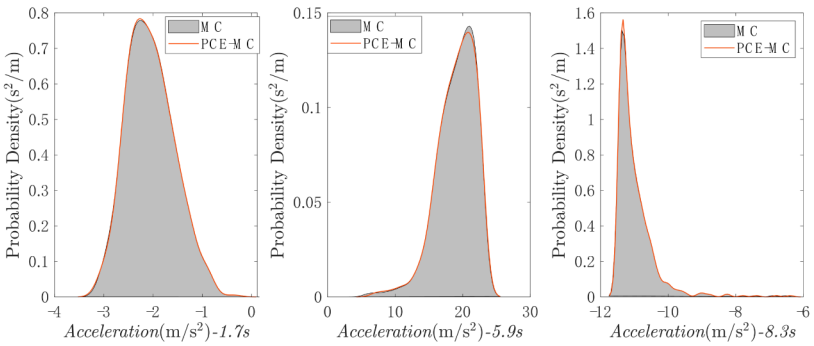

(a) Body acceleration distribution

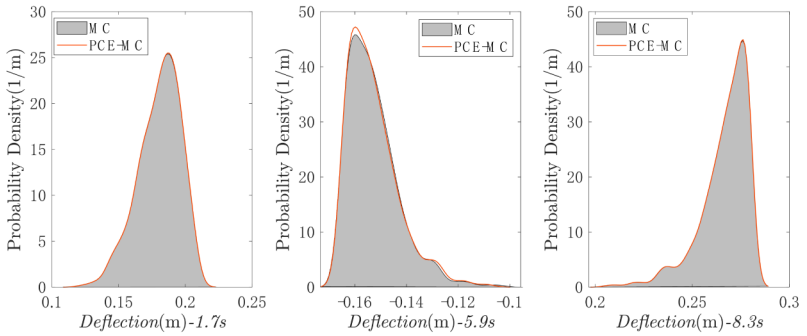

(b) Suspension dynamic deflection distribution

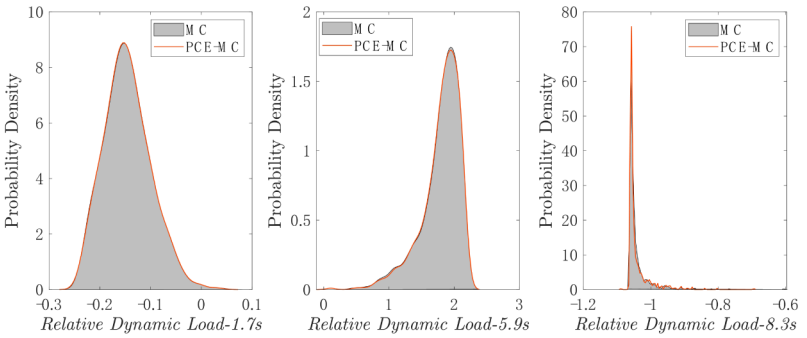

(c) Wheel relative dynamic load distribution

Figure 13 Distribution of output random variables

To compare the effects of input random variables with different variation coefficients on the response of system, two different coefficients of variation (10%, 20%) were selected. The mean and variance of the response of three random variables on the output of the system are obtained by the PCE method under the excitation of sinusoidal and step signals, respectively.

Figures 14, 15 and 16 show the effect of random variables with different coefficients of variation on the a, f_d, and F_d/G responses. The variation coefficients of the random input parameters are chosen to be 10% and 20%. Figure 14(a) shows the random responses of body acceleration. It can be seen that when the variation coefficients of the random variable are 0.1, the effect differences of

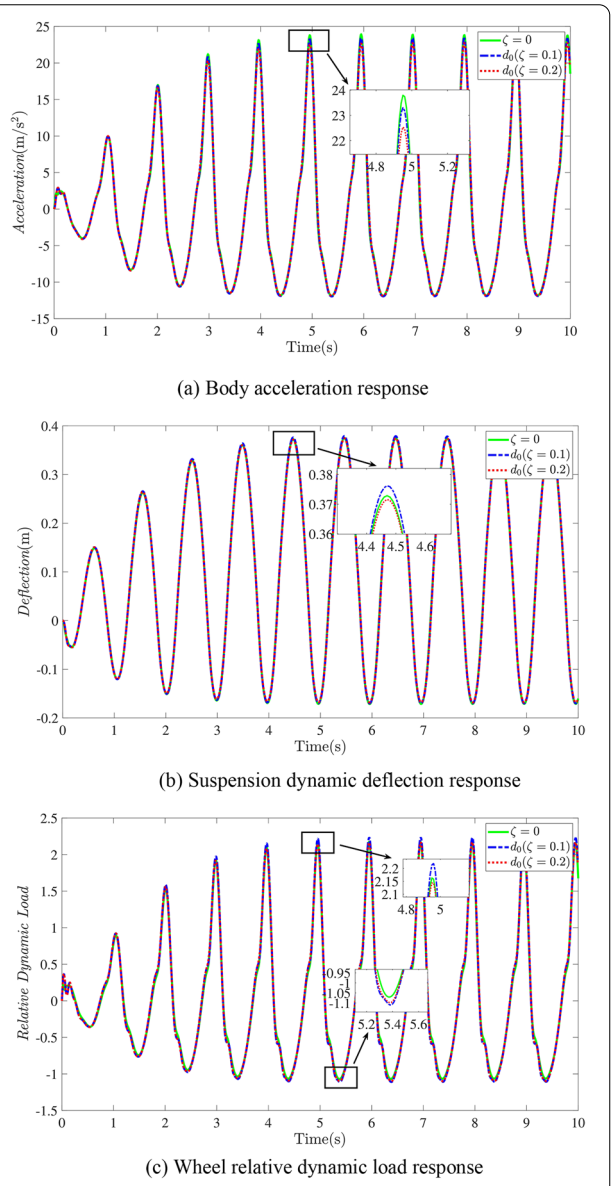

(a) Body acceleration response

(b) Suspension dynamic deflection response

(c) Wheel relative dynamic load response

Figure 14 Effect of d_0 with different coefficients of variation on the mean values of the responses under sinusoidal road excitation input

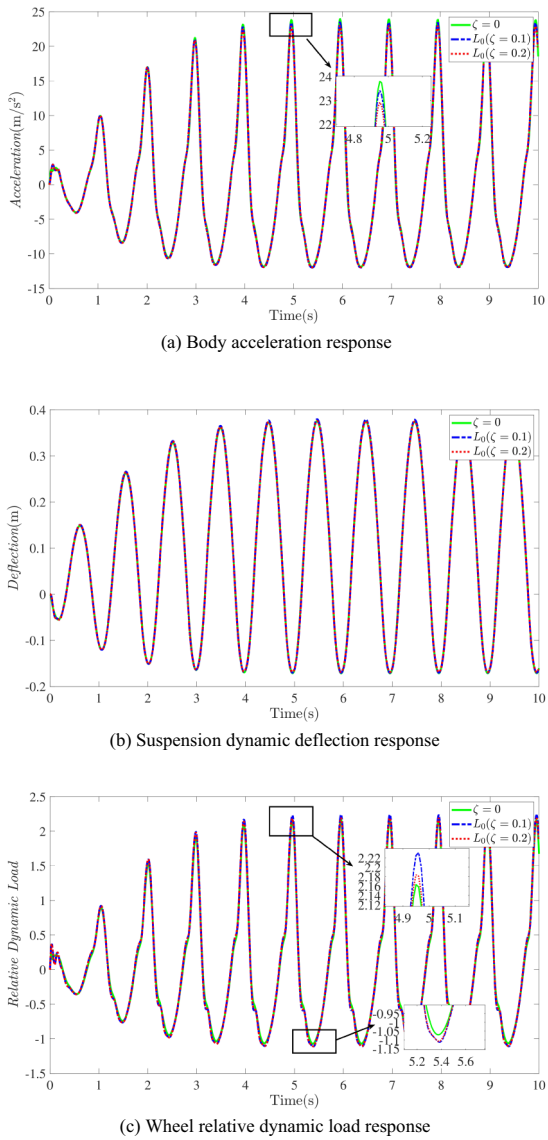

(a) Body acceleration response

(b) Suspension dynamic deflection response

(c) Wheel relative dynamic load response

Figure 15 Effect of L_0 with different coefficients of variation on the mean values of the responses under sinusoidal road excitation input

d_0 and L_0 on the mean value of the body acceleration responses is not significant, and the effect of P_{c0} is greater than that of other random variables, and the highest point of the curve is the highest point of the $\zeta = 0$ curve. That means the output response of the random variable mean is not equal to the mean of the output response. The mean response curve of the suspension dynamic deflection is given by Figures 14(b), 15(b) and 16(b), which shows that P_{c0} is still the most significant random variable affecting the mean value of the system output. 20% variation coefficient of P_{c0} is the smallest amplitude among all the curves. The other curves have more similar characteristics to Figures 14(a), 15(a) and 16(a). The mean of F_d/G responses are shown in Figures 14(c), 15(c) and 16(c), and the same by Figure 16 is that P_{c0} with 20% coefficient of variation is the smallest amplitude among all the curves. This also illustrates that the output response of the system analyzed with the design value as input can show a large deviation due to the uncertainty of the parameters. Different random variables can have different effects on the system response.

To further quantify the random variables, the response mean-maximum (RMM) and response variance mean (RVM) are defined as indexes for evaluating the effect

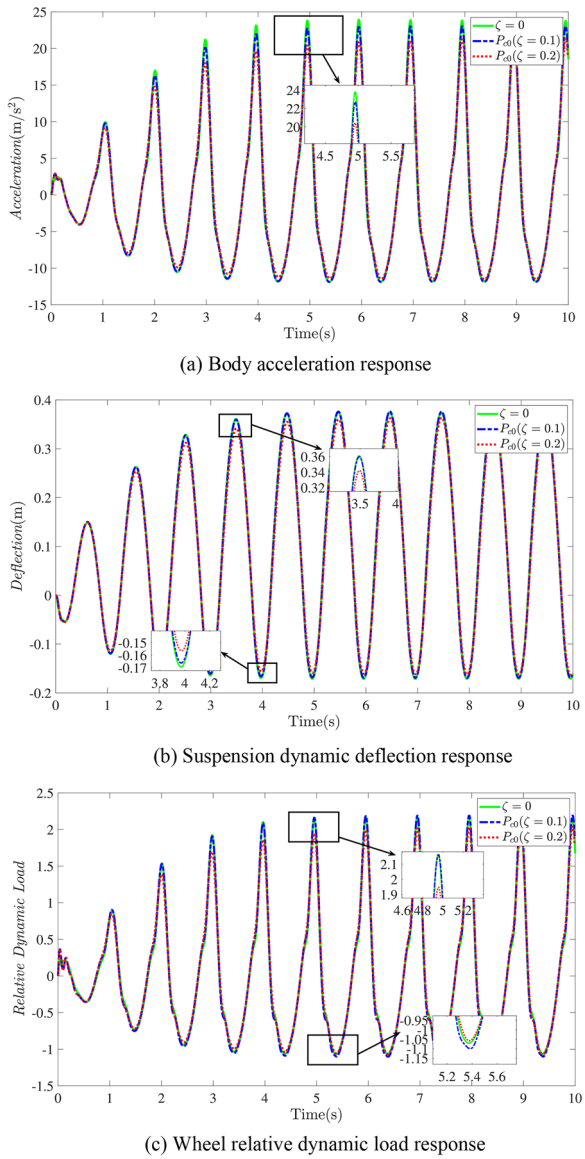

(a) Body acceleration response

(b) Suspension dynamic deflection response

(c) Wheel relative dynamic load response

Figure 16 Effect of P_{c0} with different coefficients of variation on the mean values of the responses under sinusoidal road excitation input

of input random variables on the output response under sinusoidal road excitation. The RMM is calculated by finding the maximum value of the output response mean,

Table 4 Body acceleration RMM (m/s^2), RVM (m^2/s^4) induced by random variable inputs with different coefficients of variation

Input random variables	$\zeta = 10\%$		$\zeta = 20\%$	
	RMM	RVM	RMM	RVM
d_0	23.4278	0.6113	22.7419	2.3366
L_0	23.4799	0.3698	22.9516	1.4444
P_{c0}	23.0401	1.9468	21.3869	7.5703

Table 5 Dynamic deflection of suspension RMM (m), RVM (m^2) induced by random variable inputs with different coefficients of variation

Input random variables	$\zeta = 10\%$		$\zeta = 20\%$	
	RMM	RVM	RMM	RVM
d_0	0.3784	0.0001	0.3740	0.0006
L_0	0.3785	0.0001	0.3748	0.0004
P_{c0}	0.3760	0.0004	0.3618	0.0021

Table 6 Wheel relative dynamic load RMM, RVM induced by random variable inputs with different coefficients of variation

Input random variables	$\zeta = 10\%$		$\zeta = 20\%$	
	RMM	RVM	RMM	RVM
d_0	2.2355	0.0060	2.1707	0.0228
L_0	2.2436	0.0037	2.1948	0.0144
P_{c0}	2.1957	0.0190	2.0164	0.0701

and the RVM is obtained by averaging the response variance at each simulated output point. The magnitudes of RMM and RVM for body acceleration with different input random variables at different variation coefficients ζ are given in Table 4. And the RMM equals to 23.9361 m/s^2 when the body acceleration under deterministic input. By comparison, it is found that the RMM of acceleration under random input is smaller than that under deterministic input. The effects of the random variable d_0 and L_0 on the random variable acceleration a are closer under the same coefficient of variation. However, the effect of L_0 is smaller than that of d_0, and the variance of the output response is also the smallest. The output response is most sensitive to P_{c0} under the same variation coefficient. The body acceleration response due to P_{c0} as a random variable input changes the most with respect to the deterministic input for both RMM and RVM. The corresponding RMM and RVM changes when the variation coefficient increases, and the RVM increases more significantly. Accordingly, the output response is more dispersed, but the RMM shows a slight decrease. Similarly, the RMM and RVM of the suspension dynamic deflection are also calculated in this paper. The value of its RMM is 0.3754 m under the deterministic input, as shown in Table 5. All three random variable inputs have a small effect on the RMM of the output response. As the same as the body acceleration, P_{c0} as the random variable input causes the largest change in the response and generate the more dispersed output relative to the other two variables. The change in the variation coefficient ζ from 10% to 20% causes a 4−6 times change in the RVM, and

it can be seen that the variation coefficient ζ can have a greater effect on the dispersion of the output response. Table 6 gives the response of the last output response, wheel dynamic load, for different random input variables, and it can be seen that the effect on the output is $P_{c0} > d_0 > L_0$. Similarly, the increase of ζ causes the output variable distribution to be more dispersed.

It is essential to pass a speed bump when vehicle driving on a city road, or suddenly a tire presses over a stone on a country road. In these cases, the performance of the vehicle suspension directly affects the smoothness and safety of the vehicle. This paper also studies the influence of the parameters' uncertainties on the vehicle suspension performance under the step road

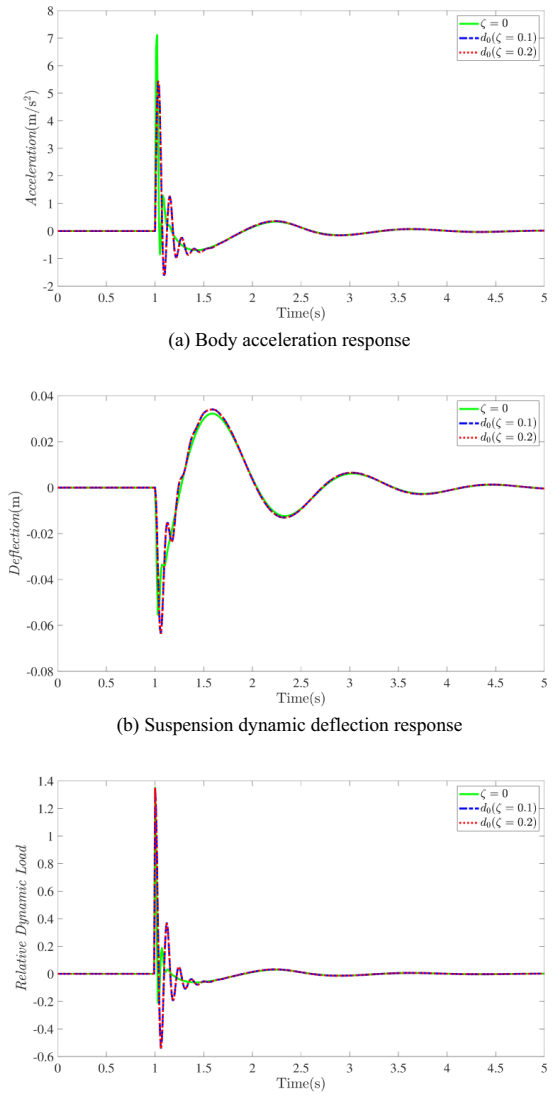

(a) Body acceleration response

(b) Suspension dynamic deflection response

(c) Wheel relative dynamic load response

Figure 17 Effect of d_0 with different coefficients of variation on the mean values of the responses under sinusoidal road excitation input

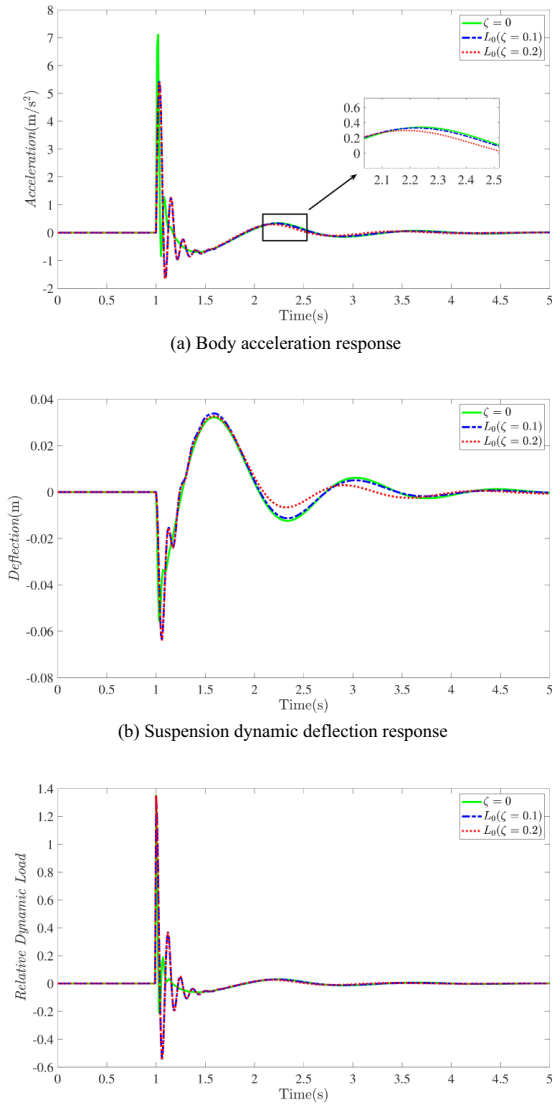

(a) Body acceleration response

(b) Suspension dynamic deflection response

(c) Wheel relative dynamic load response

Figure 18 Effect of L_0 with different coefficients of variation on the mean values of the responses under sinusoidal road excitation input

excitation, Figures 17, 18 and 19 show the vehicle body acceleration, suspension dynamic deflection, and wheel dynamic load response with time when the road surface is a step signal. It can be seen from Figures 17(a), 18(a) and 19(a) that the effect of different inputs on the body acceleration is not significant enough, but there is still a small difference. The body acceleration can recover to zero value faster when the coefficient of variation of P_{c0} is 20%. From Figures 17(b), 18(b) and 19(b), the mean suspension dynamic deflection output is more sensitive to the difference of the variation coefficient and parameters. There is an anomaly, that is, P_{c0} and L_0 are always in the position of greater than zero after 2.5 s when

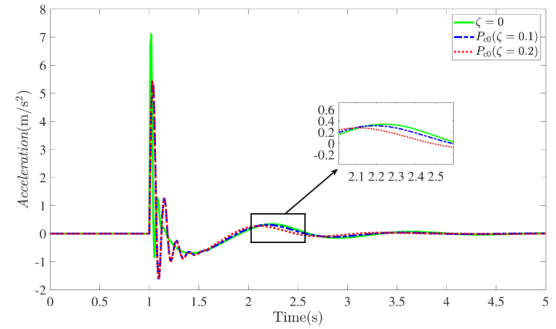

(a) Body acceleration response

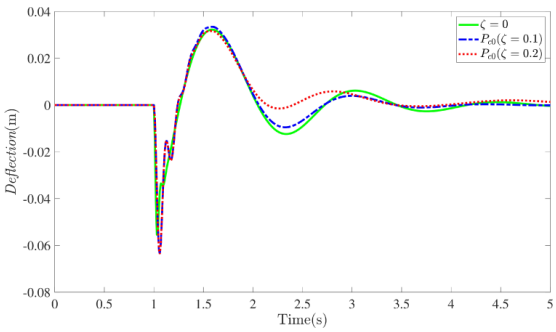

(b) Suspension dynamic deflection response

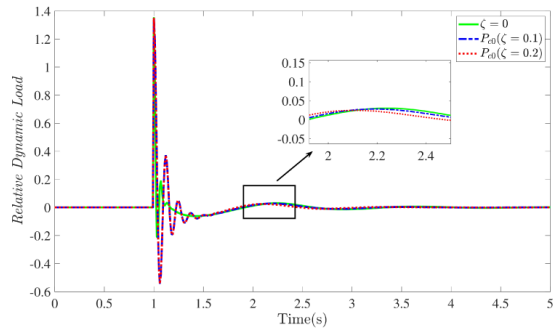

(c) Wheel relative dynamic load response

Figure 19 Effect of P_{c0} with different coefficients of variation on the mean values of the responses under sinusoidal road excitation input

the variation coefficient ζ is 20%, which means that the deflection cannot recover to the original equilibrium position. And Figures 17(c), 18(c) and 19(c) show that the wheel relative dynamic load F_d/G is more insensitive to the difference between the random variables and the coefficient of variation relative to the other two performance parameters.

For a random road surface which the vehicle travels normally, the road velocity spectrum $\sqrt{\dot{G}_q(\omega)}$ is white noise, and the root-mean-square value spectrum of the responses such as body acceleration, suspension dynamic deflection, and wheel relative dynamic load is

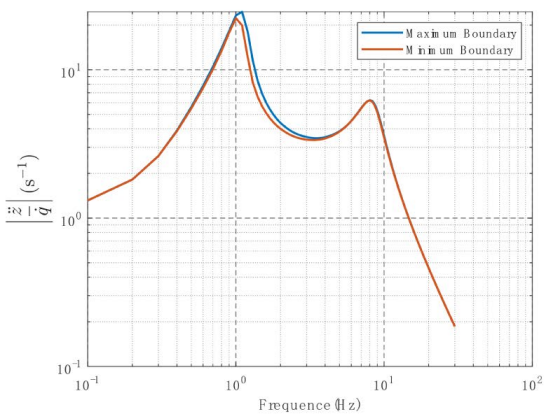

(a) Body acceleration response

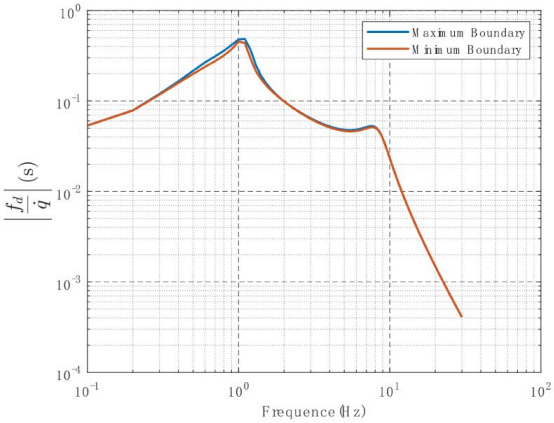

(b) Suspension dynamic deflection response

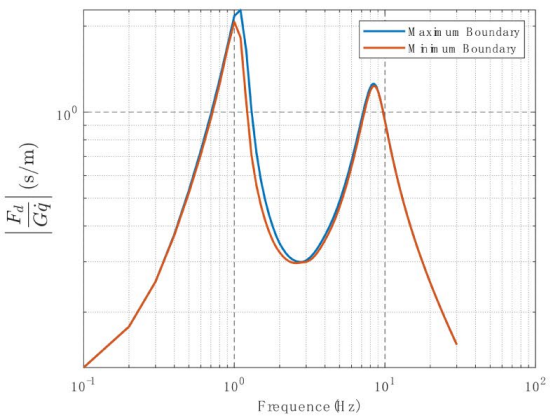

(c) Wheel relative dynamic load response

Figure 20 Effect of d_0 uncertainty on a, f_d, and F_d/G vs. $\dot{q}$ amplitude-frequency characteristics

the amplitude-frequency characteristic multiplied by the constant $\sqrt{\dot{G}_q(\omega)}$. So that one can use the amplitude-frequency characteristics of the response volume

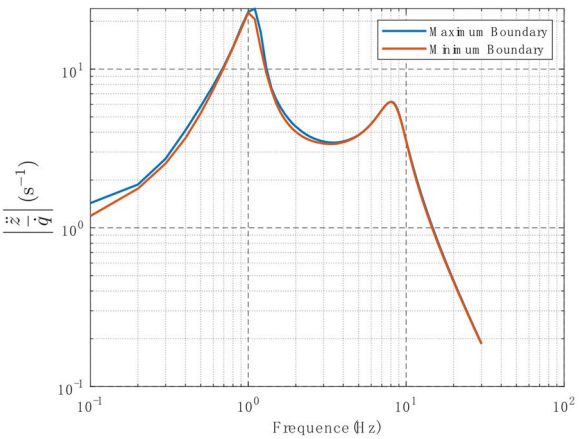

(a) Body acceleration response

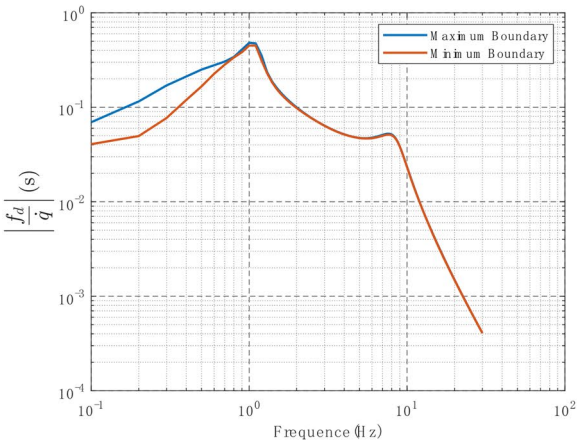

(b) Suspension dynamic deflection response

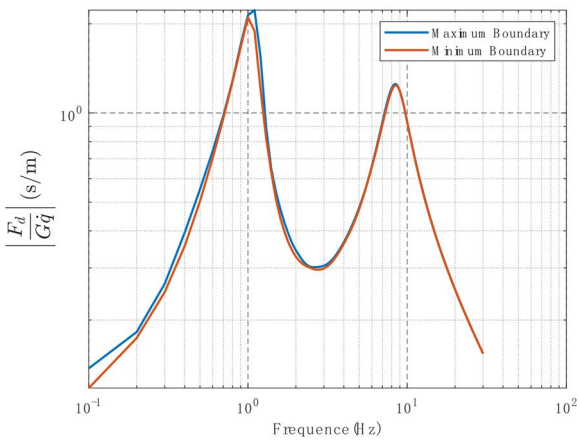

(c) Wheel relative dynamic load response

Figure 21 Effect of L_0 uncertainty on a, f_d, and F_d/G vs. $\dot{q}$ amplitude-frequency characteristics

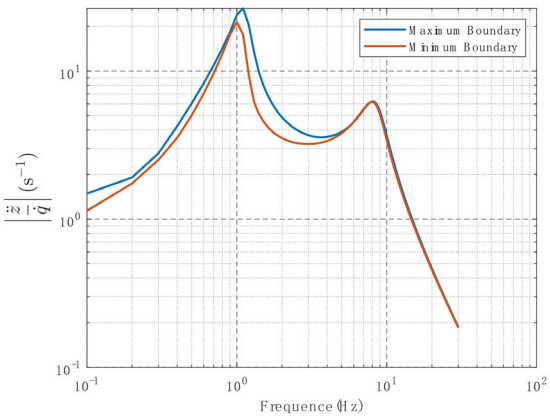

(a) Body acceleration response

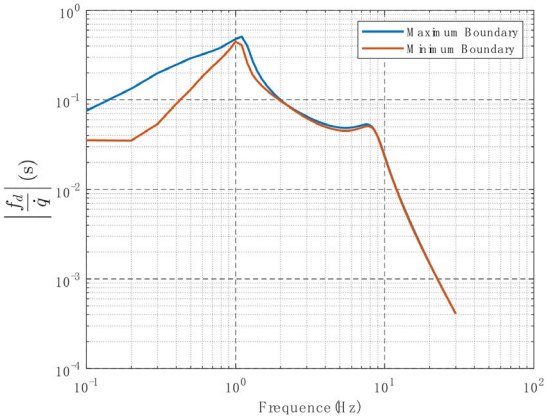

(b) Suspension dynamic deflection response

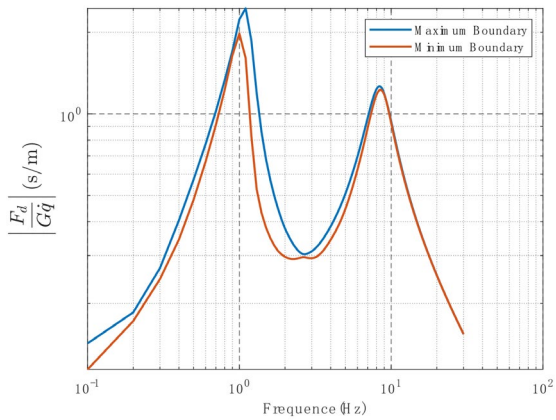

(c) Wheel relative dynamic load response

Figure 22 Effect of P_{c0} uncertainty on a, f_d, and F_d/G vs. $\dot{q}$ amplitude-frequency characteristics

to the velocity input to qualitatively analyze the root-mean-square value spectrum of the response.

Figures 20, 21 and 22 show the upper and lower bound of the amplitude-frequency characteristics of the response volume to velocity input obtained by using the

PCE method. The variation coefficient of the random variables was all taken as 10%, and the magnitudes of the upper and lower bound curves were obtained by adding and subtracting twice the standard deviation from the derived mean value.

From Figure 20(a), it can be concluded that at frequencies less than 1 Hz, the maximum and minimum bounds almost coincide.

In the low frequency band, the uncertainty of d_0 has almost no effect on the magnitude-frequency characteristics. When the frequency is in the range of 1−4 Hz, the maximum and minimum bound curves are not in coincidence, and most of the magnitudes fluctuate within the maximum and minimum bounds due to the uncertainty of d_0. When the frequency is greater than 4 Hz, the two curves overlap and the effect of d_0 uncertainty on the amplitude-frequency characteristics becomes minor. As a comparison, Figure 21(a) shows the amplitude-frequency characteristic curves of L_0 as an input random variable. Unlike Figure 20(a), the difference between the maximum and minimum bounds is larger in the low frequency band. The uncertainty of L_0 in the low frequency region has a greater effect on the acceleration compared to d_0. And the range of amplitude frequency response caused by L_0 in the middle frequency band of 1−10 Hz is smaller than the range caused by d_0 in Figure 20(a), which indicates that the body acceleration response is more sensitive to d_0 than L_0 in the middle frequency band. When the frequency is greater than 10 Hz, there is almost no difference between the curves of the two plots. The effect of P_{c0} on the response is given by Figure 22(a). Comparing the other two plots, the difference between the maximum and minimum boundary curves is the largest in both the low-frequency and the mid-frequency regions. It can be concluded that the uncertainty of P_{c0} has the largest effect on the body acceleration among three random variables. In the high frequency region, there is almost no difference between the effects of three random variables.

Figures 20(b), 21(b), and 22(b) give the effects of three random variables on suspension dynamic deflection, respectively. The influence region caused by d_0 uncertainty is mainly between 0.3 and 2 Hz, the influence region of P_{c0} is within 1 Hz, and P_{c0} has a large influence on suspension dynamic deflection up to 2 Hz, but the influence is more significant in the low frequency region. By comparison, it is found that in the low frequency region with frequency less than 0.8 Hz, the influence level of uncertainty arranges as $P_{c0} > L_0 > d_0$, and in the middle frequency 0.83 Hz, the influence level of uncertainty arranges as $P_{c0} > d_0 > L_0$. At other frequency band, the three random variables have the same influence level.

For the dynamic wheel load, it can be seen from Figures 20(c), 21(c), and 22(c) that the influence region caused by d0 uncertainty is mainly between 1−10 Hz, the influence region of P_{c0} is within 4 Hz, and P_{c0} has a greater influence on the dynamic suspension deflection up to 10 Hz, but the influence is more significant in the intermediate frequency region. By comparison, it is found that in the low frequency region with frequency less than 1 Hz, the influence level of uncertainty arranges as $P_{c0} > L_0 > d_0$, and in the intermediate frequency 1−5 Hz, the influence level of uncertainty arranges as $P_{c0} > d_0 > L_0$. Three random variables have close influence level at higher frequency band.

5 Uncertainty Optimization Using NSGA-II

The parameters of QZSAS are related to the vibration isolation performance of the whole system, and it can be seen from the above section that the uncertainties generated by the QZSAS parameters due to manufacturing and installation tolerance, changes in ambient temperature, wear and tear of the mechanical structure and sensor errors will cause more or less changes in the suspension performance parameters. Therefore, the suspension performance response is also a distribution rather than a specific value. In order to evaluate the suspension performance, the mean value is used to reflect the overall merit of performance and the standard deviation to reflect the dispersion of the performance, because it is also unreasonable if the optimization results make the suspension performance index too dispersed. Therefore, the RMS value of acceleration is used as the optimization target, and the parameters d_0, L_0, and P_{c0} of QZSAS are optimized under the common class B road surface. And their coefficients of variation are all taken as 0.1, the distribution is shown in Figure 11. Therefore, the optimization target is divided into two parts, the first part is the mean value of the RMS value of acceleration, and the other part is the standard deviation of the RMS value of acceleration, so that the overall comfort performance of QZSAS is ensured, and the comfort will not have a large deviation. Thus, the whole optimization process can be expressed by the following equation:

$$\min\ \mu_a,\ \sigma_a, \tag{20}$$

$$\text{s.t.}\quad \begin{cases} 200\ \text{kPa} \le P_{c0} \le 600\ \text{kPa}, \\ 0.3\ \text{m} \le L_0 \le 0.7\ \text{m}, \\ 0.02\ \text{m} \le d_0 \le 0.05\ \text{m}. \end{cases} \tag{21}$$

NSGA-II is used to optimize the quasi-zero stiffness air suspension parameters. NSGA-II algorithm, the fast

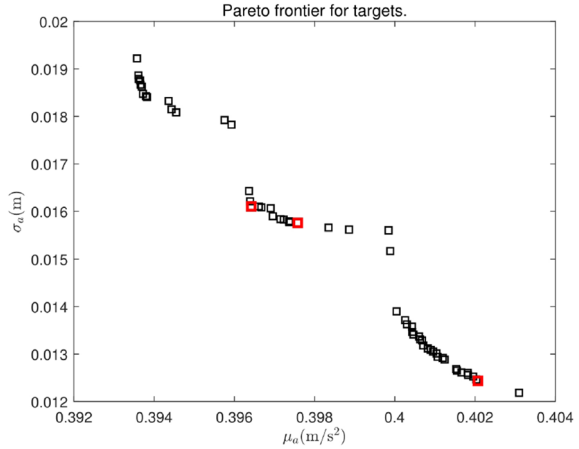

Figure 23 Pareto frontier for targets

non-dominated multi-objective optimization algorithm with elite retention strategy, is a multi-objective optimization algorithm based on the Pareto optimal solution. The key step in the whole optimization process is to establish the relationship between the optimization design parameters and objectives. The output of the fitness function is an indicator to assess the fitness of the population.

Another key step in NSGA-II is the selection of the pareto-optimal individual, which is simply explained as the Pareto-optimal individual if no individual exists for which any of the objectives is superior to the current individual.

The Pareto dominance relation is defined as follows: for a minimization multi-objective optimization problem, for n objective components $f_i(x)$ $(i = 1, 2,..., n)$. Given any two decision variables X_a and X_b, X_a is said to dominate X_b if the following two conditions hold:

Table 7 Initial design point and optimized points

Points	P	P1	P2	P3
d_0(m)	0.0325	0.0337	0.0265	0.0380
L_0(m)	0.467	0.4896	0.4768	0.4919
P_{c0}(kPa)	300	415	406	403

1. $\forall i \in \{1, 2, ..., n\}, f_i(X_a) \leq f_i(X_b)$,
2. $\exists i \in \{1, 2, ..., n\}, f_i(X_a) < f_i(X_b)$.

A decision variable is said to be a non-dominated solution if there are no other decision variables that can dominate it.

Pareto rank: In a set of solutions, the Pareto rank of the non-dominated solution is defined as 1. By removing the non-dominated solution from the set of solutions, the Pareto rank of the remaining solutions is defined as 2, and so on, the Pareto ranks of all solutions in the set of solutions can be obtained.

The Pareto front of the suspension performance is shown in Figure 23. The performance points on the Pareto front are essentially equivalent, with each point being optimal until the two performance indices are weighted. For example, a point with a smaller μ_a must have a larger σ_a than another point.

The Pareto optimal solution set is shown in Figure 24. It can be seen that the optimized parameters are not in the middle of the optimization space. It can be seen that they are concentrated on the right side of the space and appear as long strips. The d_0 of the optimal solution presents a dispersed form, which also coincides with the small effect of d_0 on the suspension performance in the previous section. The P_{c0} of the optimal solution is fairly concentrated around 400 kPa. The L_0 of the optimal solution is also more concentrated and ranges from 0.48 to

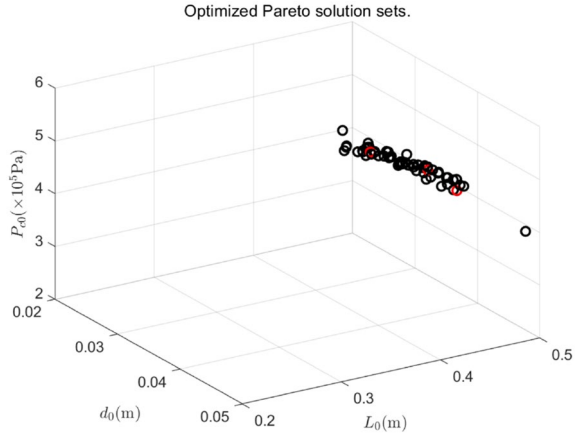

Figure 24 Optimized Pareto solution sets

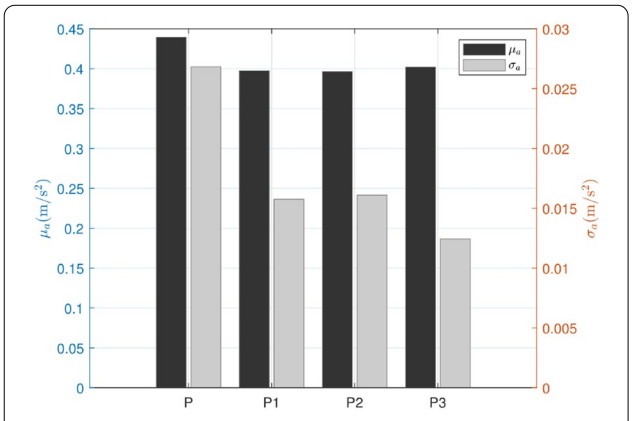

Figure 25 Objective values before and after optimization

Table 8 Objective values before and after optimization

Objects	P	P1		P2		P3	
	Values	Values	Upgrades (%)	Values	Upgrades (%)	Values	Upgrades (%)
μ_a	0.4394	0.3976	9.51	0.3964	9.77	0.4021	8.49
σ_a	0.0268	0.0158	41.26	0.0161	39.97	0.0124	53.65

0.5 m. The reason for this result could be the different sensitivity of the acceleration of the suspension to each parameter.

In an attempt to visually compare the effect before and after optimization, three Pareto optimal solutions for every weight and the initial design point P have been selected to compare the target performance indices. Three optimal Pareto solutions (P1, P2, P3) with their corresponding ground indices have been marked in red in Figure 23, and their coordinates are shown in Table 7. Figure 25 shows the standard deviation and mean value of acceleration (RMS) before and after optimization. It can be seen that both the standard deviation and mean value have decreased, and the decline degree of standard deviation is particularly significant. The details of the improvement values are recorded in Table 8. The optimization results show that there is an improvement of about 8%−10% in the mean value and about 40%−55% in the standard deviation of acceleration values (RMS).

6 Conclusions

In this paper, PCE method is applied to the QZSAS to analyze the effects of parameters uncertainties on suspension performance. The uncertainty parameters chosen in this paper are structural parameters of the suspension. The output responses were selected suspension performance parameters. The main conclusions are included as follows.

(1) By comparing with the MC method, it is found that the PCE method is feasible in solving the uncertainty problem and can produce results very close to those of the MC method.
(2) Although the input variables follow a normal distribution, the distribution of the output responses is not a symmetrically but a skewed distribution.
(3) The output response distributions of the suspension are related to input random variables, the variation coefficient of the inputs, and road profile excitation. The sensitivity of the suspension performance parameters to different frequency road surfaces is different. The influence level of each structural parameter is focused on a certain frequency band.
(4) A multi-objective optimization of the structural parameters of QZSAS was performed with the mean and variance of the RMS acceleration values as the optimization objectives. There is an improvement in both the mean value and standard deviation of acceleration values (RMS).

This paper provides a theoretical basis for the design and optimization of suspensions. It is of practical importance to consider the uncertainties of parameters when designing a suspension. The mean value of the output performance parameters reflects the overall effect of the suspension design, and the standard deviation reflects the ability of the suspension to maintain performance. In the process of design and optimization, both mean and standard deviation must be considered for the superior performance of the suspension.

Acknowledgements
Not applicable.

Authors' Contributions
XX proposed the structure of the quasi-zero stiffness air suspension, also he pointed out the direction of the research and established the main structure of this paper. HL and XJ were responsible for programming the polynomial chaos method and building the model, and AVA was responsible for checking the self-consistency of the logic and the correctness of the English grammar in the paper. All authors read and approved the final manuscript.

Authors' Information
Xing Xu, born in 1979, is currently a professor at *Automotive Engineering Research Institute, Jiangsu University, China*. He received his PhD degree from *Jiangsu University, China,* in 2010. His research interests include vehicle dynamics control, energy storage system for alternative vehicles.
Huan Liu, born in 1996, is currently a master candidate at *Automotive Engineering Research Institute, Jiangsu University, China*.
Xinwei Jiang, born in 1993, is currently a PhD candidate at *Automotive Engineering Research Institute, Jiangsu University, China*.
Akolbire Vincent Atindana, born in 1983, obtained his bachelor's and master's degrees in automotive engineering at *Kwame Nkrumah University of Science and Technology (Ho-Poly Campus)* and *University of Education-Winneba, Ghana*. He is a Lecturer at *Tamale Technical University, Ghana*. And he is currently a PhD candidate at *Automotive Engineering Research Institute, Jiangsu University, China*.

Funding
Supported by National Natural Science Foundation of China (Grant No. 51875256), Open Platform Fund of Hunan Institute of Technology of China (Grant No. KFA20009) and Hong Kong, Macao and Taiwan Science and Technology Cooperation Project in Jiangsu Province of China (Grant No. BZ2020050).

Competing Interests
The authors declare no competing financial interests.

Received: 29 June 2021 Revised: 26 May 2022 Accepted: 1 June 2022
Published online: 14 July 2022

References

[1] E Palomares, A J Nieto, A L Morales, et al. Numerical and experimental analysis of a vibration isolator equipped with a negative stiffness system. *Journal of Sound and Vibration*, 2018, 414: 31-42.
[2] S Yuan, Y Sun, J Zhao, et al. A tunable quasi-zero stiffness isolator based on a linear electromagnetic spring. *Journal of Sound and Vibration*, 2020, 482(6):115449.
[3] P M Alabuzhev, A Gritchin. *Vibration protecting and measuring systems with quasi-zero stiffness*. Hemisphere Publishing Co. , Taylor & Francis Group, 1989.
[4] G Yan, H X Zou, S Wang, et al. Large stroke quasi-zero stiffness vibration isolator using three-link mechanism. *Journal of Sound and Vibration*, 2020, 478:115344.
[5] Y Jiang, C Song, C Ding, et al. Design of magnetic-air hybrid quasi-zero stiffness vibration isolation system. *Journal of Sound and Vibration*, 2020, 477:115346.
[6] T D Le, K K Ahn. Experimental investigation of a vibration isolation system using negative stiffness structure. *International Journal of Mechanical Sciences*, 2013, 70(5): 99-112.
[7] F Zhao, J C Ji, K Ye, et al. Increase of quasi-zero stiffness region using two pairs of oblique spring. *Mechanical Systems and Signal Processing*, 2020, 144:106975.
[8] F Ling, Z Y Ma, Z F Tang, et al. Uncertainty analysis of vehicle suspension systems based on polynomial chaos methods. In *Proceedings of 2013 4th International Conference on Intelligent Systems Design and Engineering Applications*, ISDEA, 2013, 732-735.
[9] D S Yoon, G W Kim, S B Choi. Response time of magnetorheological dampers to current inputs in a semi-active suspension system: modeling, control and sensitivity analysis. *Mechanical Systems and Signal Processing*, 2021, 146:106999.
[10] Z Nagy, R Braatz. Distributional uncertainty analysis using polynomial chaos expansions. In *Proceedings of the IEEE International Symposium on Computer-Aided Control System Design*, 2010: 1103-1108.
[11] M Dodson, G T Parks. Robust aerodynamic design optimization using polynomial chaos. *Journal of Aircraft*, 2015, 46(2): 635-646.
[12] [12] J Dai, G Wei, N Zhang. Random displacement and acceleration responses of vehicles with uncertainty. *Journal of Mechanical Science & Technology*, 2011, 25(5): 1221-1229.
[13] C Ke, X Yu, H Zheng, et al. Study on the unascertained-dynamic model and dynamic response of vehicle suspension. *Chinese Journal of Applied Mechanics*, 2017, 34(4): 647-653+812. (in Chinese)
[14] N Wiener. The homogeneous chaos. *American Journal of Mathematics*, 1938, 60(4): 897-936.
[15] F Schneider, I Papaioannou, M Ehre, et al. Polynomial chaos based rational approximation in linear structural dynamics with parameter uncertainties. *Computers & Structures*, 2020, 233:106223.
[16] D Shi, X Fang, F Holzapfel. Polynomial chaos-based flight control optimization with guaranteed probabilistic performance. *IFAC-PapersOnLine*, 2020, 53(2): 7274–7279.
[17] A Sandu, C Sandu, M Ahmadian. Modeling multibody systems with uncertainties. Part I: Theoretical and computational aspects. *Multibody System Dynamics*, 2006, 15(4): 369-391.
[18] X Jiang, S Li, R Furfaro, et al. High-dimensional uncertainty quantification for Mars atmospheric entry using adaptive generalized polynomial chaos. *Aerospace Science and Technology*, 2020, 107:106240.
[19] D Métivier, M Vuffray, S Misra. Efficient polynomial chaos expansion for uncertainty quantification in power systems. *Electric Power Systems Research*, 2020, 189:106791.
[20] G Kewlani, J Crawford, K Iagnemma. A polynomial chaos approach to the analysis of vehicle dynamics under uncertainty. *Vehicle System Dynamics*, 2012, 50(5):749-774.
[21] C Qiu, X Peng, Z Y Liu. Sensitivity analysis of random and interval uncertain variables based on polynomial chaos expansion method. *IEEE Access*, 2019, 7:73046-73056.
[22] Y Chen, M Ahmadian, A Peterson. Pneumatically balanced heavy truck air suspensions for improved roll stability. *SAE Technical Papers*, 2015, 2015-01-2749.
[23] Y Chen, M Ahmadian. Countering the destabilizing effects of shifted loads through pneumatic suspension design. *SAE International Journal of Vehicle System Dynamics, Stability and NVH*. 2019, 4(1):5-17.
[24] C D Jayaweera, M Narayana. Multi-objective dynamic optimization of seeded suspension polymerization process. *Chemical Engineering Journal*, 2021, 426:130797.
[25] S Li, J Xu, H Gao, et al. Safety probability based multi-objective optimization of energy-harvesting suspension system. *Energy*, 2020, 209(12):118362.
[26] M P Nagarkar, Y J Bhalerao, G J V Patil, et al. Multi-objective optimization of nonlinear quarter car suspension system – PID and LQR control. *Procedia Manufacturing*, 2018, 20:420-427.
[27] G Papaioannou, D Koulocheris. Multi-objective optimization of semi-active suspensions using KEMOGA algorithm. *Engineering Science and Technology, an International Journal*, 2019, 22(4): 1035-1046.
[28] B Gadhvi, V Savsani, V Patel. Multi-objective optimization of vehicle passive suspension system using NSGA-II, SPEA2 and PESA-II. *Procedia Technology*, 2016, 23:361-368.
[29] D Xiu. Efficient collocational approach for parametric uncertainty analysis. *Communications in Computational Physics*, 2007, 2(2): 293-309.
[30] S S Isukapalli. *Uncertainty analysis of transport-transformation models*. New Jersey: The State University of New Jersey, 1999.

Submit your manuscript to a SpringerOpen journal and benefit from:

► Convenient online submission
► Rigorous peer review
► Open access: articles freely available online
► High visibility within the field
► Retaining the copyright to your article

Submit your next manuscript at ► springeropen.com